Photolabeling Study of the Ligand Binding Domain of Natriuretic Peptide Receptor A: Development of a Model†

Christian Jossart,‡ Martin Coupal,§ Normand McNicoll,‡ Alain Fournier,§ Brian C. Wilkes,|| and André De Léan*,‡,⊥

Département de Pharmacologie, Faculté de Médecine, Université de Montréal, Montréal, Québec, Canada, Centre de Recherche en Santé Humaine, INRS-Santé/Institut Armand-Frappier, Université du Québec, Pointe-Claire, Québec, Canada, and Institut de Recherches Cliniques de Montréal, Montréal, Québec, Canada

Received August 13, 2004; Revised Manuscript Received October 27, 2004

ABSTRACT: Atrial natriuretic peptide (ANP) and brain natriuretic peptide (BNP) are loop-shaped peptidic hormones that have multiple actions on body fluid homeostasis. Their physiological effects are mediated through the activation of their receptor, natriuretic peptide receptor A (NPRA). This receptor is a member of the membrane guanylyl cyclase family and catalyzes cyclic guanosine monophosphate (cGMP) production following its activation. To map the binding site of human NPRA, we applied the methionine proximity assay method to this receptor. We photolabeled NPRA mutants, presenting a single methionine in the binding domain of the receptor, and used benzoylphenylalanine- (Bpa-) substituted peptides at positions 0, 3, 18, 26, and 28 of the ligand. We identified that the N-terminus of the peptide is interacting with the region between Asp^{177} and Val^{183} of the receptor. Arg^3 is interacting in the vicinity of Phe^{172}. Leu^{18} binds close to Val^{116}. Phe^{26} binds in the vicinity of His^{195}, and the C-terminal Tyr^{28} is located close to Met^{173}. We next proceeded with photolabeling of a dual Bpa-substituted peptide and showed that the N-terminus and Leu^{18} interact with opposite receptor subunits. On the basis of our results, a molecular model of peptide-bound NPRA was developed by homology modeling with the C-type natriuretic peptide- (CNP-) bound natriuretic peptide receptor C (NPRC) crystal structure. The model has been validated by molecular dynamics simulations. Our work provides a rational basis for interpreting and predicting natriuretic peptide binding to the human NPRA.

Natriuretic peptides are hormones secreted by the heart in response to blood overload. They modulate body fluid homeostasis by increasing natriuresis, diuresis, and vasorelaxation and by inhibiting aldosterone secretion (*1*−*3*). They also inhibit cell hypertrophy (*4*) and proliferation (*5*). These peptides mediate their effects by activating the production of the second messenger cyclic GMP, following their binding to guanylyl cyclase receptors (*6*). Because of its multiple positive cardiovascular effects, the natriuretic peptide nesiritide is now used as a therapeutic agent for the treatment of congestive heart failure (*7*). Natriuretic peptide receptors belong to the particulate guanylyl cyclase family. Natriuretic peptide receptor A (NPRA)[1] and natriuretic peptide receptor B (NPRB) are sometimes referred to as GC-A and GC-B, respectively (*8*).

Atrial natriuretic peptide (ANP), brain natriuretic peptide (BNP), and C-type natriuretic peptide (CNP) are the main natriuretic peptides. They share a common ring structure formed by a disulfide bond between two conserved cysteine residues. These peptides contain N- and C-terminal sequences that extend from the common ring structure, except for CNP, which is devoid of a C-terminal tail (*9*). ANP and BNP display high affinity for NPRA (*10*), whose activation causes natriuresis, diuresis, and vasorelaxation. CNP binds preferentially NPRB (*11*) to elicit mainly vasorelaxing effects. Natriuretic peptide receptor C (NPRC) binds all three peptides with high affinity (*10*) but is devoid of any catalytic domain. NPRC is thought to act as a clearance receptor by controlling local concentration of free peptides (*12*).

NPRA and NPRB share a very similar noncovalent homodimeric structure typical of particulate guanylyl cyclases. They consist of a glycosylated extracellular domain (ECD) containing the peptide binding site, a single transmembrane (TM) domain, a constitutively phosphorylated kinase homology domain that presumably binds ATP, a coiled-coil dimerization domain, and a catalytic guanylyl cyclase domain (*13*). NPRC is quite different. It is a covalent disulfide-bridged dimer with an ECD and a TM but only a short intracellular segment (*14*). This intracellular segment

† This work was supported by grants from the Canadian Institutes for Health Research.

* To whom correspondence should be addressed: Département de Pharmacologie, Faculté de Médecine, Université de Montréal, C. P. 6128, Centre-Ville, Montréal, H3C 3J7, Canada. Tel 514-343-6931; fax 514-343-2291; e-mail delean@pharmco.umontreal.ca.

‡ Université de Montréal.

§ Université du Québec.

|| Institut de Recherches Cliniques de Montréal.

⊥ Recipient of a Research Chair from Merck Frosst Canada.

[1] Abbreviations: ANP, atrial natriuretic peptide; ATP, adenosine triphosphate; BNP, brain natriuretic peptide; Bpa, *p*-benzoyl-L-phenylalanine; cGMP, cyclic guanosine monophosphate; CNP, C-type natriuretic peptide; ECD, extracellular domain; EDTA, ethylenediaminetetraacetic acid; HPLC, high-performance liquid chromatography; MPA, methionine proximity assay; NPRA, natriuretic peptide receptor A; NPRC, natriuretic peptide receptor C; PAGE, polyacrylamide gel electrophoresis; SDS, sodium dodecyl sulfate; TM, transmembrane; WT, wild type.

10.1021/bi048251y CCC: $30.25
Published on Web 01/28/2005

might also mediate signaling since it has been shown to interact with Gi proteins (*15, 16*).

The extracellular domain of rat NPRA has been crystallized in the absence of ligand (*17*). The structure of each subunit displayed a bilobed type I periplasmic-binding protein folding. A dimerization interface was initially proposed to be located in the membrane-proximal lobe, leading to a V-shaped receptor conformation. This structure was compatible with two ANP binding sites, one located on the lateral face of each subunit, suggesting a 2:2 stoichiometric ratio, in agreement with Misono et al. (*18*) but in contrast with a 1:2 ratio documented by Rondeau et al. (*19*). Crystallization of the ECD for human NPRC in both the CNP-bound and the unliganded forms clarified this ambiguity (*20*). Despite a periplasmic-binding protein folding pattern similar to that for NPRA, the dimerization interface for NPRC was located in the membrane-distal lobe of each subunit, yielding an A-shaped receptor dimer. A single CNP molecule was bound in the center of the 2-fold symmetric dimer. CNP adopted a disklike conformation inserted in the intersubunit cleft below the dimerization interface, contributing to the interaction between two receptor monomers. Binding of the peptide induces membrane-proximal lobes to close by approximately 13 Å, squeezing the peptide in the receptor (*20*). The 1:2 stoichiometric ratio of natriuretic peptide binding was further confirmed by microcalorimetric studies (*20*). More recently, dimerization studies and cross-linking experiments in the distal lobe of NPRA with bifunctional agents established that NPRA also adopts the same A-shaped dimer conformation (*21*). These results were then confirmed later by site-directed mutagenesis (*22*). Finally, the crystal structure of an A-shaped rat NPRA ECD bound to a truncated ANP[7−27] has been recently published (*23*). The structure obtained by that group, including the lateral rotation of the subunits for the ligand-bound form, confirmed the results previously reported for the CNP−NPRC complex (*20*), including the 1:2 stoichiometric ratio of ANP to NPRA subunit.

Our knowledge of the NPRA ligand binding site still remains incomplete. However, photolabeling studies are well-known to yield valuable data on receptor binding sites. Benzophenones are one of the most efficient tools for photoaffinity labeling. Bpa (*p*-benzoyl-L-phenylalanine), a nonnatural amino acid, is the most popular example. Bpa is substituted in peptidic hormones by organic synthesis and has the ability to cross-link efficiently and selectively with other amino acids when activated by UV light (*24*). It reacts with electron-rich C−H bonds, for example, backbone carbons, C_β-H of valine, Cγ-H of leucine, and methylenes adjacent to heteroatoms in lysine, arginine, and methionine (*24*). Methionine is the most reactive amino acid and it can be labeled by Bpa if they are located within a 6−7 Å radius of each other (*25*). Bpa has been used to localize the binding site of several receptors including neurokinin-1 receptor (*26*) and angiotensin AT_1 (*27*) and AT_2 (*28*) receptors. The method has been applied to natriuretic peptides and the development of highly efficient labeling probes for NPRA opened the way for the characterization of the peptide binding domain (*29*). We have previously shown that dimerization with a bifunctional photoaffinity derivative of the peptide that it is interacting with both subunits of the receptor (*19*). The ligand binding site of NPRA was then studied with two different photolabeling probes. One was cross-linked to the receptor through the N-terminus of the peptide with UV-generated malondialdehyde, and the other labeled the receptor through its Bpa-containing C-terminus (*30*). The former labeled a fragment corresponding to the region between Met^{173} and Phe^{188}, while the latter labeled the segment Asp^{191}−Arg^{198} of NPRA.

With the emergence of new strategies in benzophenone photolabeling experiments, we are now able to better define the binding site of a peptidic hormone with accuracy. By using the methionine proximity assay (MPA) as a guideline (*25*), we introduced by site-directed mutagenesis a single methionine at the surface of the ligand binding domain of NPRA. Several Bpa derivatives of the chimeric peptide (N,C-rANP)pBNP (*31*), a superagonist more potent than ANP on human NPRA (*32*), have been prepared (*33*). The site of covalent bonding between the Bpa-containing peptides and methionines in the receptor was documented by CNBr cleavage and SDS−PAGE analysis. CNBr has the property to cleave not only the protein backbone at the C-terminal of methionines but also the photolabeled Bpa-substituted peptide attached to the terminal methyl group of the methionine side chain (*26*). This yields a distinctive low molecular band on SDS−PAGE when a methionine is labeled (*26*). On the basis of these results, a molecular model of peptide-bound NPRA was developed by using homology modeling, starting with the CNP-bound NPRC crystal structure (*20*). These results provide a rational basis for interpreting and predicting natriuretic peptide binding to their human receptor.

EXPERIMENTAL PROCEDURES

Construction of Human NPRA Mutants. The wild-type (WT) human NPRA cloned into PBS-KS(−) vector was generously provided by David G. Lowe (Genentech). By use of the Transformer mutagenesis kit (Clontech), a *Sma*I site had been inserted 20 nt after the stop codon with the mutagenic primer 5′-CTCCTATCCCGGGACACCTCCC-3′. The vector was then subcloned into the pBK-CMV vector (Stratagene) by use of sites *Xba*I and *Sma*I. The construction was validated by sequencing. $NPRA^{M173L}$ was obtained by use of the QuikChange site-directed mutagenesis kit (Stratagene) with the oligonucleotide 5′-GTGGAGGGGCTGT-TCTTAAGGGTCCGCGACCGCC-3′ and its complementary sequence. The fragment encompassing the mutation between *Sgr*AI and *Eco*RV sites was subcloned into $NPRA^{WT}$, and the construction was validated by sequencing. All other NPRA mutants were derived from $NPRA^{M173L}$ by the same QuikChange procedure. For all these mutants, the fragment between *Sgr*AI and *Eco*RV sites was subcloned into $NPRA^{WT}$ and the construction was validated by sequencing.

Cell Culture and Transfection. Human embryonic kidney cells line 293 (HEK 293) (American Type Culture Collection) were grown in Dulbecco's modified Eagle's medium supplemented with 10% fetal bovine serum and 100 units of penicillin/streptomycin in a 5% CO_2 incubator at 37 °C. Cells (1.4×10^6) were plated on 100 mm plates and transfected following the $CaHPO_4$ precipitation method as described previously (*38*).

Membrane Preparations. Membrane from transfected HEK 293 cells were prepared according to Labrecque et al. (*39*) Briefly, cells were harvested 72 h after transfection and

homogenized in ice-cold buffer A (10 mM Tris-HCl, pH 7.4, 1 mM EDTA, 1 μM aprotinin, 1 μM leupeptin, 1 μM pepstatin, and 10 μM Pefabloc) with a Polytron homogenizer. The homogenate was centrifuged at 35000*g* for 30 min and pellets were washed twice with buffer A. Finally, membranes were resuspended in ice-cold freezing buffer B (50 mM Tris-HCl, pH 7.4, 0.1 mM EDTA, 1 mM $MgCl_2$, 250 mM sucrose, and proteases inhibitors) and stored at −80 °C until used. Total protein concentrations were determined with the BCA protein assay kit (Pierce).

Peptide Synthesis of Bpa Analogues. All peptides were synthesized by solid-phase peptide synthesis (*40*) on a homemade manual multireactor system. Chloromethylated resin (Bio-Rad Laboratories) served as solid support. Couplings were carried out with 3 equiv of BOP reagent (Richelieu Biotechnologies), 3 equiv of Boc-AA-OH, and 5 equiv of diisopropylethylamine (Aldrich). Monitoring of residue addition was achieved through the ninhydrin test (*41*). Amino acid side-chain deprotection, as well as peptide cleavage from the solid support, were achieved through use of liquid hydrogen fluoride. All analogues were purified by reverse-phase HPLC on a DeltaPak C_{18} reverse-phase column and individual fractions were analyzed by analytical HPLC on a Vydac C_{18} reverse-phase column as described previously (*33*).

Addition reaction for dual Bpa-substituted analogue pBNP1-I was performed by incubating the single Bpa analogue (pBNP1-F) at a concentration of 250 μM in reaction buffer (50 mM NaH_2PO_4 and 100 mM NaCl, pH 7.4) with 1 mM of 4-benzoylbenzoic acid *N*-hydroxysuccinimide ester (Sigma) and incubating for 3 h at room temperature. Acetonitrile and trifluoroacetic acid were then added at final concentrations of 15% and 0.7%, respectively. pBNP1-I was purified by reverse-phase HPLC on a Vydac C_{18} column as described above.

Peptide Iodination and Receptor Binding Assay. Peptides were radioiodinated with $Na^{125}I$ by the lactoperoxidase method as described elsewhere (*42*). Competition experiments were performed by incubating 3−10 μg of membrane preparation with 10 fmol of ^{125}I-rANP and increasing concentrations of nonradioactive peptides in 1 mL of binding buffer (50 mM Tris-HCl, pH 7.4, 0.1 mM EDTA, 5 mM $MnCl_2$, and 0.5% bovine serum albumin) during 90 min at room temperature. Bound ^{125}I-rANP was separated from free ligand by filtration on Whatman GF/C filters pretreated with a 1% polyethylenimine solution. Filters were washed with 4 × 4 mL of 50 mM KH_2PO_4 buffer, pH 7.4, and counted in a LKB γ counter. Curves were analyzed with the program AllFit for Windows based on the four-parameter logistic equation (*43*).

Photoaffinity Labeling. Membranes were incubated in the dark with 100 fmol of ^{125}I-pBNP1−Bpa in 1 mL of vacuum degassed photolabeling buffer (50 mM Tris-HCl, pH 7.4, 0.1 mM EDTA, 5 mM $MgCl_2$, and 0.5% bovine serum albumin) for 90 min at room temperature. To each tube was added 10 μL of 10 mM PABA, and photolabeling was performed on ice by irradiation with two mercury UV lamps (365 nm) for 15 min. Tubes were vortexed twice during irradiation. Membranes were finally centrifuged at 12000*g* for 20 min and pellets were resuspended in Laemmli sample buffer (62 mM Tris-HCl, pH 6.8, 2% SDS, 10% glycerol, 5% β-mercaptoethanol, and 0.001% bromophenol blue) and denatured at 100 °C for 4 min.

Partial Purification of the Labeled Receptor. Photolabeled proteins were purified by SDS−7.5% PAGE. The gel was cut into 2.5 mm slices and the band corresponding to the labeled receptor was detected in a γ counter. The selected band was passively eluted in 10 volumes of 0.1% SDS/50 mM NH_4HCO_3 and dried down in a SpeedVac concentrator. For radiolabeling with the dual Bpa-substituted pBNP1-I, the bands corresponding to the monomeric and dimeric receptors were cut off the gel and measured in a γ counter without further treatment.

Chemical Cleavage and Enzymatic Digestions. For CNBr cleavage, the amount of radioactive receptors was usually normalized to 1000 cpm. The photolabeled receptor was resuspended in 100 μL of 70% formic acid containing 100 mg/mL CNBr. Proteins were incubated for 20 h at 22 °C in the dark. The digestion medium was diluted with 10 volumes of water and concentrated twice in a SpeedVac concentrator. For Asp-N digestion, the partially purified photolabeled receptor was resuspended in a buffer containing 50 mM NaH_2PO_4, 1 M urea, and 20 mM CH_3NH_2, pH 8.0, and heated at 60 °C for 30 min. After cooling, the enzyme (Sigma) was added for a 1 μg/mL final concentration and the sample was incubated for 20 h at 37 °C. For carboxypeptidase A digestion, 150 nmol of peptide (pBNP1-A) was evaporated and resuspended in 0.5 mL of digestion buffer (0.2 M NH_4HCO_3, pH 8.5). Agarose-coupled carboxypeptidase A gel (100 μL; Sigma) was prewashed twice with 0.4 mL of digestion buffer and was added to the peptide. The mix was incubated for 30 min at 37 °C with agitation. After centrifugation, the digested peptide was recovered and purified on a Vydac C_{18} column as described earlier.

Electrophoresis and Autoradiography. Samples were resuspended in polypeptide sample buffer (50 mM Tris-HCl, pH 6.8, 4% SDS, 12% glycerol, 2% β-mercaptoethanol, and 0.01% Serva Blue G) and loaded on an SDS−Tris−tricine−16.5% polyacrylamide gel according to Schägger and von Jagow (*44*). Protein fragments were transferred onto a nitrocellulose membrane (Bio-Rad) in 25 mM Tris-HCl, 192 mM glycine, and 20% methanol via the liquid Trans-Blot system (Bio-Rad), and radiolabeled fragments were detected by autoradiography.

Homology Modeling of hNPRA Dimer Complexed to pBNP1. All calculations were performed with the software package SYBYL 6.91 (Tripos Associates, St. Louis, MO). The Tripos force field was used for energy calculations and a dielectric constant of 1 was used. The X-ray crystal structure of CNP bound to the NPRC dimer (*20*) was used as a template for the receptor-bound form of hNPRA, and the corrected X-ray crystal structure of rNPRA without a ligand (*17*) was used as a template for the open form of hNPRA. All external water molecules and other counterions were removed, except for the essential buried chloride ions, and the complexes were subjected to 1000 steps of energy minimization. By use of the sequence alignment of van den Akker (*45*), each variable amino acid within the receptor dimer complex was replaced one at a time by its equivalent in hNPRA sequence. The backbone dihedral angles were held fixed to preserve the receptor's secondary structure, while the amino acid side chains were positioned by use of the scan subroutine in SYBYL. This routine rotates each side-

Table 1: Primary Structures of rANP, pBNP, the Related Chimeric Analogue pBNP1, and Synthesized Photoaffinity Labeling Probes[a]

peptide	name	structure
rat ANP	ANP	SLRRSSCFGGRIDRIGAQSGLGCNSFRY
porcine BNP	BNP	SPKTMRDSGCFGRRLDRIGSLSGLGCNVLRRY
(*N*,*C*-rANP)pBNP	pBNP1	SLRRSSCFGRRLDRIGSLSGLGCNSFRY
[N^{α}-*p*-benzoylbenzoyl,Tyr^{2}]pBNP1	pBNP1-A	*p*-benzoylbenzoyl-SYRRSSCFGRRLDRIGSLSGLGCNSFRY
[N^{α}-*p*-benzoylbenzoyl,Tyr^{18}]pBNP1	pBNP1-B	*p*-benzoylbenzoyl-SLRRSSCFGRRLDRIGSYSGLGCNSFRY
[Tyr^{2},Bpa^{3}]pBNP1	pBNP1-C	SYBRSSCFGRRLDRIGSLSGLGCNSFRY
[Tyr^{6},Bpa^{9}]pBNP1	pBNP1-D	SLRRSYCFBRRLDRIGSLSGLGCNSFRY
[Bpa^{16},Tyr^{18}]pBNP1	pBNP1-E	SLRRSSCFGRRLDRIBSYSGLGCNSFRY
[Bpa^{18},Tyr^{26}]pBNP1	pBNP1-F	SLRRSSCFGRRLDRIGSBSGLGCNSYRY
[Tyr^{18},Bpa^{26}]pBNP1	pBNP1-G	SLRRSSCFGRRLDRIGSYSGLGCNSBRY
[Tyr^{18},Bpa^{28}]pBNP1	pBNP1-H	SLRRSSCFGRRLDRIGSYSGLGCNSFRB
[N^{α}-*p*-benzoylbenzoyl,Bpa^{18},Tyr^{26}]pBNP1	pBNP1-I	p-benzoylbenzoyl-SLRRSSCFGRRLDRIGSBSGLGCNSYRY

[a] Substituted amino acids are underlined. Bpa residues are designed by the letter B.

chain dihedral angle until a sterically acceptable conformation was obtained. Gaps within the sequence alignment were dealt with by one of two methods. When the gap required the removal of 1−3 amino acids, they were excised and a new amide bond was formed. The dihedral angle of the new amide bond was fixed at 180°, and the complex was minimized to relieve the resulting strain and allow the resulting gap to close. When the gap required the addition of 1−3 amino acids, the required amide bond was broken, a distance constraint was applied of 3 Å per amino acid to be added, and the complex was minimized to allow the amino acids to move apart. The necessary amino acids were then placed in the resulting gap in a random conformation and new amide bonds were formed. Again the complex was minimized, allowing all atoms to relax. After all the required transformations were complete, the complex was again minimized for 1000 steps. No major conformational changes were observed during the minimization process. Modeling of pBNP1 bound to the receptor-bound form of hNPRA was performed stepwise. The core of pBNP1, consisting of residues 6−22, which contains the cyclic portion of the molecule, was modeled on the basis of the conformation of CNP found in the CNP−NPRC complex. As before, each amino acid was transformed one amino acid at a time and scanned to obtain a sterically acceptable conformation. Placement of the N-terminal residues 1−5 and the C-terminal residues 23−28 was based on the contact points found by use of the photoaffinity results of this work. Both backbone and side-chain dihedral angles of these residues were manipulated until steric complementarity with the receptor dimer was obtained and the required ligand to receptor contact was formed. At this point the complex was again subjected to 1000 steps of minimization. To construct pBNP1 bound to the open form of hNPRA, the resulting conformation of pBNP1 was excised from the receptor-bound form of hNPRA and attached to one monomer of the open form of the hNPRA dimer, preserving all contacts found with the receptor-bound form of the receptor. This structure was also minimized for 1000 steps.

Molecular Dynamics. Molecular dynamics simulations were performed on both the receptor-bound and open forms of hNPRA, both with and without pBNP1 bound. Each of the four simulations was for 300 ps at 300 K. Movement of the two monomers of the receptor dimer relative to each other was monitored by measuring the distance between Arg^{208} of each monomer during the dynamics simulations.

RESULTS

Development of High-Efficiency Photolabeling Probes. A photoaffinity scan with Bpa-substituted analogues of pBNP1 was carried out in order to document efficient probes for our present topographical mapping study. The hybrid peptide pBNP1 is derived from rat ANP termini and porcine BNP ring sequences (*31*). This peptide was previously documented as the one with highest potency for human NPRA (*32*). Using solid-phase peptide synthesis, we created five pBNP1 analogues with Bpa at different positions (Table 1). Bpa substitution positions were selected according to structure−activity relationship studies for ANP identifying Phe^{8}, Ile^{12}, Asp^{13}, Arg^{14}, Ile^{15}, Leu^{21}, and Arg^{27} as ligand binding-dependent residues (*34*, *35*). Those residues were not Bpa-substituted for this reason. An additional tyrosine was also inserted in order to track radioiodinated CNBr fragments. Their positions were based on surface accessibility shown by NMR studies of pBNP1 (*36*) and NMR modeling of the hexamutant ANP (*37*). We included two previously tested probes (*33*) in our labeling experiments, pBNP1-A and pBNP1-B (Table 1). These two *p*-benzoylbenzoyl-derived probes were selected in order to achieve a more complete study of the N-terminus. The potency and cross-linking specificity of the peptide analogues were tested on membrane preparations of NPRA (data not shown). All but pBNP1-D maintained high affinity, and therefore pBNP1-D was rejected as a probe. pBNP1-E displayed high affinity for NPRA but did not covalently label the receptor, suggesting that its Bpa side chain is not pointing toward the receptor. No further studies were performed with this peptide. We selected pBNP1-A, -B, -C, -F, -G, -H and -I for further studies since they all possessed high affinity, at least equipotent to ANP binding to hNPRA, and a sufficiently high cross-linking incorporation yield.

Development of Single-Methionine NPRA Mutants. Wild-type human NPRA contains Met^{173} as the only exposed methionine in the binding domain, based on the corrected A-shaped rNPRA crystal structure (*45*) and previous photolabeling results (*30*). Using site-directed mutagenesis, we substituted Met^{173} with leucine in order to yield the mutant $NPRA^{M173L}$ devoid of an exposed methionine in the binding domain. $NPRA^{M173L}$ displayed no significant loss of affinity for ANP and was used as a reference for further receptor mutants (data not shown). In an attempt to identify sites susceptible to Bpa reaction, we then introduced methionines in the binding domain of $NPRA^{M173L}$. The residues that were

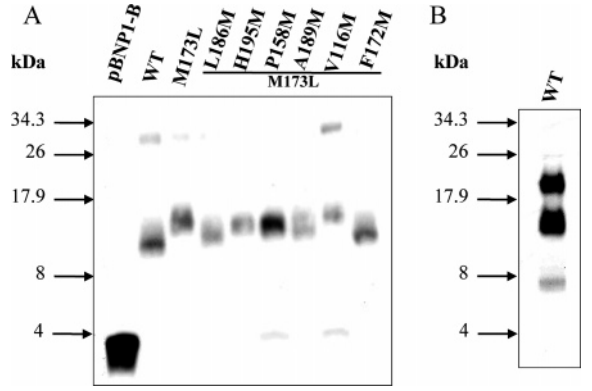

FIGURE 1: SDS−PAGE analysis of photolabeling with pBNP1-A and pBNP1-B probes. (A) Photolabeling with pBNP1-B. NPRA receptors were incubated with radioiodinated pBNP1-B and submitted to photoaffinity labeling as described under Experimental Procedures. The labeled receptors were isolated on an SDS−polyacrylamide gel and then subjected to CNBr cleavage. The resulting polypeptides were resuspended in sample buffer and loaded on an SDS−Tris−tricine−16.5% polyacrylamide gel. The 11 kDa band in the WT lane and the 12 kDa band in the M173L−L186M lane are identifying the Arg^{174}−Leu^{186} region of the receptor for probe labeling. Results are representative of two independent experiments. (B) Photolabeling with pBNP1-A[1−27]. Wild-type NPRA was incubated with radioiodinated pBNP1-A[1−27] and submitted to photoaffinity labeling. The complex was isolated on an SDS−polyacrylamide gel and subjected to Asp-N proteinase digestion. The resulting polypeptidic fragments were loaded on an SDS−Tris−tricine−16.5% polyacrylamide gel. The 8 kDa band identifies the Asp^{177}−Val^{183} region of the receptor for probe labeling. Results are representative of four independent experiments.

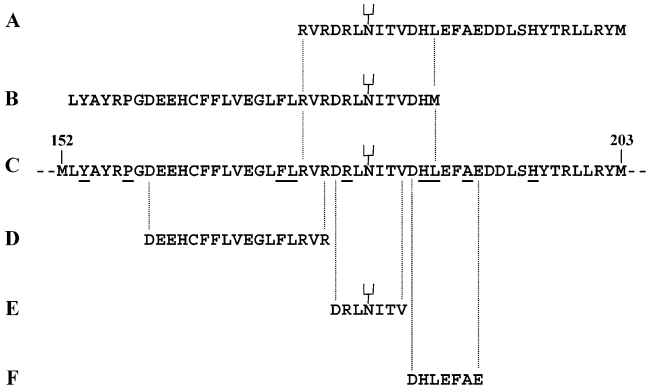

FIGURE 2: Protein sequence of the binding domain of human NPRA. Mutated residues are underlined. Glycosylated Asn^{180} is identified. (A) Sequence of the Arg^{174}−Met^{203} region deduced from CNBr cleavage of pBNP1-B-labeled $NPRA^{WT}$. (B) Sequence of the Leu^{153}−Leu^{186} region deduced from CNBr cleavage of pBNP1-B-labeled $NPRA^{M173L-L186M}$. (C) Sequence of the Leu^{153}−Met^{203} region deduced from CNBr cleavage of pBNP1-B-labeled $NPRA^{M173L}$. (D−F) Illustration of the possible fragments generated by Asp-N proteolysis of NPRA.

chosen were hydrophobic or polar and had to be exposed in the rNPRA structure. The following receptor mutants were prepared: $NPRA^{M173L-L186M}$, $NPRA^{M173L-H195M}$, $NPRA^{M173L-P158M}$, $NPRA^{M173L-A189M}$, $NPRA^{M173L-V116M}$, $NPRA^{M173L-F172M}$, $NPRA^{M173L-Y154M}$, and $NPRA^{M173L-H185M}$. The hormone binding properties of those receptor mutants have been investigated. Mutations Y154M and H185M were found to abrogate receptor binding. Other receptor mutants showed only marginal affinity decrease (data not shown) and were therefore used for the following photolabeling experiments.

N-Terminus of pBNP1 Binds in Region between Asp^{177} and Val^{183}. Our first experiments were intended to find a contact point for the N-terminal of the peptide. Membrane preparations expressing our NPRA mutants and WT receptor were incubated with the radioiodinated pBNP1-B probe and subjected to photoaffinity labeling as described under Experimental Procedures. The labeled receptors were isolated by elution from an SDS−polyacrylamide gel and submitted to CNBr cleavage. The fragment mixtures were dried and then loaded on an SDS−Tris−tricine−16.5% polyacrylamide gel (Figure 1A). None of the CNBr-cleaved receptor mutants yielded a major 4 kDa band, suggesting that none of the iodinated probes were released by CNBr. This observation suggests that the N-terminus of pBNP1 is located at least at a 6 Å distance from all methionines. It is also possible that the N-terminal of pBNP1 is too mobile to stay in the neighborhood of a methionine long enough to react. Still, the fragments yielded by CNBr cleavage can be interpreted since this agent also cleaves the protein backbone at the C-terminal side of methionines. For M173L mutant, the fragment radiolabeled by pBNP1-B migrates as a 13 kDa band. This labeled fragment could be identified as corresponding to the Leu^{153}−Met^{203} region (Figure 2C). This region is characterized by a N-glycosylation of Asn^{180} (*42*). All other receptor mutants labeled by pBNP1-B yielded bands ranging from 10.5 to 13 kDa. These fragments all correspond to a region encompassed within the Leu^{153}−Met^{203} fragment, but their lengths fluctuate depending on the position of the substituted methionine. The 11 kDa band observed for the WT receptor corresponds to the Arg^{174}−Met^{203} region (Figure 2A), while the 12 kDa band from the M173L−L186M mutant corresponds to the Leu^{153}−Leu^{186} region (Figure 2B). Those two intersecting fragments define the common labeled sequence Arg^{174}−Leu^{186}. Photolabeled bands found with other receptor mutants localize to the same Leu^{153}−Met^{203} region, which also includes the Arg^{174}−Leu^{186} sequence. These results demonstrate that the peptide N-terminus labels the receptor between Arg^{174} and Leu^{186}.

While both pBNP-A and pBNP-B contain a *p*-benzoylbenzoyl group at the N-terminus, pBNP-A differs from pBNP-B in the position of the tyrosine residue (Table 1). This characteristic allows for enzymatic digestion of labeled receptor without losing the radioactive signal from the peptide. To leave only one iodination site on pBNP1-A, we pretreated this probe with carboxypeptidase A. This enzyme removed the tyrosine residue at the C-terminus, enabling a complete iodination only on Tyr^2. This pBNP1-A[1−27] peptide retained its full affinity for NPRA (data not shown). In an attempt to define a more precise region labeled by the N-terminus, we incubated membranes expressing WT receptors with iodinated pBNP1-A[1−27] and we proceeded to photoaffinity labeling. We then digested the prepurified labeled receptor with Asp-N proteinase, which cleaves at the N-terminal side of aspartic acids, including Asp^{13} of pBNP1. The proteolytic fragments were loaded on an SDS−16.5% polyacrylamide gel (Figure 1B). The Asp-N digestion produced two major bands and a minor one. The two major bands at 14 and 20 kDa are probably resulting from incomplete digestion of the labeled receptor, since all Asp-N-digested fragments are predicted to be smaller. The minor 8 kDa band corresponds exactly to the predicted mass of the region Asp^{177}−Val^{183} (Figure 2D−F) linked to the

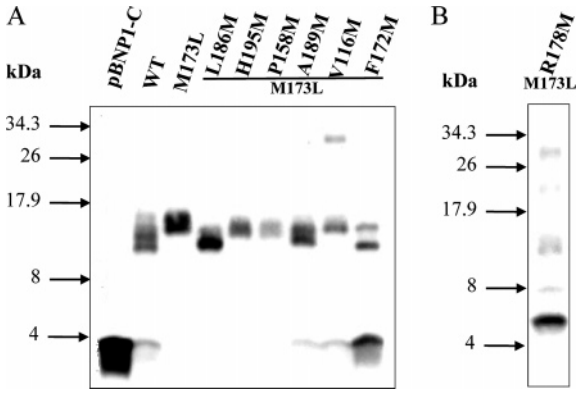

FIGURE 3: SDS−PAGE analysis of photolabeling with the pBNP1-C probe. (A) Identification of the Phe^{172} region. NPRA receptors were incubated with radioiodinated pBNP1-C and submitted to photoaffinity labeling as described in the Figure 1 caption. The 4 kDa band in the M173L−F172M lane identifies Phe^{172} as a labeling site for Bpa. Results are representative of two independent experiments. (B) Identification of the Leu^{153}−Arg^{178} region. NPRA$^{M173L-R178M}$ was incubated with radioiodinated pBNP1-C and submitted to photoaffinity labeling as described in the caption to Figure 1. The 6 kDa band identifies the Leu^{153}−Arg^{178} region of the receptor as a labeling site for Bpa. Results are representative of two independent experiments.

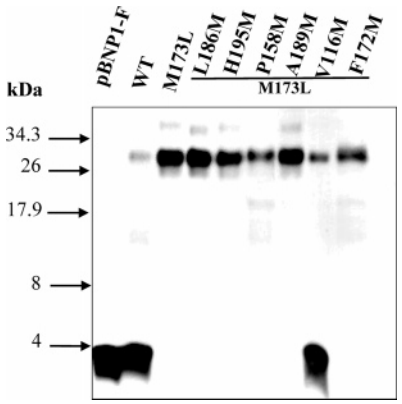

FIGURE 4: SDS−PAGE analysis of photolabeling with the pBNP1-F probe. NPRA receptors were incubated with radioiodinated pBNP1-F and submitted to photoaffinity labeling as described in the Figure 1 caption. The 28 kDa band in the M173L lane and the 4 kDa band in the M173L−V116M lane are pinpointing Val^{116} as a labeling site for Bpa. Results are representative of three independent experiments.

digested pBNP1-A[1−12], identifying this shorter region as the position for N-terminus labeling.

Arg^3 of pBNP1 Binds in the Vicinity of Phe^{172}. We then investigated the interactions of position 3 of the ligand, which is also located in the N-terminal tail of the peptide. Membrane preparations of WT and NPRA mutants were photolabeled with iodinated pBNP1-C probe. The M173L−F172M mutant (Figure 3A) shows the typical 4 kDa band associated with labeling on a methionine. It suggests that Arg^3 of pBNP1 binds in the vicinity of Phe^{172}. A minor 4 kDa band is also noticed in the WT, M173L−A189M, and M173L−V116M mutants. This suggests a proximity, but not a close contact, to Met^{173}, Ala^{189}, and Val^{116}. It might also be due to flexibility of the N-terminal tail of the probe. The 10.5−13 kDa bands yielded by other receptor mutants follow almost the same pattern as was found for pBNP1-B labeling (Figure 1A) and are all located in the same Leu^{153}−Met^{203} region. Therefore, the labeling point should be located within the common region Arg^{174}−Leu^{186}. However, the major contact point Phe^{172} also identified is located at the edge of this region, again compatible with N-terminal mobility.

To clarify this ambiguity, we tested the NPRA$^{M173L-R178M}$ mutant and confirmed that it preserved high affinity for ANP (data not shown). We then performed photoaffinity labeling of this mutant with pBNP1-C. No 4 kDa band is observed (Figure 3B), but a major 6 kDa band is obtained instead. This fragment corresponds to the Leu^{153}−Arg^{178} region, which includes Phe^{172}, while excluding a part of the Arg^{174}−Leu^{186} sequence. These results again suggest that Arg^3 interacts within the vicinity of Phe^{172} and that Arg^3 of pBNP1-C can also interact with neighboring residues in the absence of a methionine mutant. Those residues are all located between Phe^{172} and Arg^{178}. The Bpa residue appears to be much closer to Phe^{172} since a methionine substituted for Arg^{178} failed to react.

Leu^{18} of pBNP1 Binds in the Vicinity of Val^{116}. The receptor binding region of residue 18 within the peptide loop was then ascertained by photoaffinity labeling of the NPRA mutants with the iodinated pBNP1-F probe. The WT receptor and M173L−V116M mutant display a major 4 kDa band (Figure 4), suggesting a close proximity of residue 18 with the methionines at positions 173 and 116. All other mutants yield a similar 28 kDa band compatible with the Gly^1−Met^{152} portion of the receptor, which includes Val^{116}. The CNBr cleavage pattern of NPRA^{M173L} clearly shows that, in the absence of methionine, pBNP1-F preferentially cross-links the Gly^1−Met^{152} region. However the results also suggest that Met^{173}, which is present in the WT receptor and in the Leu^{153}−Met^{203} region, is also labeled by this probe. In the NPRA model, Met^{173} and Val^{116} are actually very close to each other, in agreement with this interpretation.

Phe^{26} of pBNP1 Binds in the Vicinity of His^{195}. Mapping of the position of the peptide C-terminal was obtained by photoaffinity labeling with iodinated pBNP1-G. Two 4 kDa bands are observed for the M173L−H195M and M173L−L186M mutants (Figure 5A). The band is major for His^{195} and minor for Leu^{186}. This suggests that Phe^{26} is located in the vicinity of His^{195}, not far from Leu^{186}. In fact, those residues are located close together in the rNPRA model. Two additional bands are observed for the M173L−H195M mutant. The minor 4.5 kDa fragment corresponds to the Tyr^{196}−Met^{203} region, while the 12 kDa fragment corresponds to the Leu^{153}−His^{195} region. These observations collectively suggest that His^{195} is central to the labeling zone. However, the M173L−L186M mutant also yields a 12 kDa band, indicating that the Leu^{153}−Leu^{186} region is also labeled. This also suggests that Phe^{26} could be near Leu^{186} and its surrounding residues. In addition, the M173L−A189M mutant displays a clear 5 kDa band that corresponds to the Glu^{190}−Met^{203} region, which includes His^{195}. These data demonstrates that the main labeling zone is located in the His^{195} region. The other receptor mutants yielded fragments from 10.5 to 13 kDa, as seen previously with pBNP1-B and -C and is in agreement with labeling within the Leu^{153}−Met^{203} region.

To confirm these results, we tested the NPRA$^{M173L-R198M}$ mutant, which includes Met^{198}, that is predicted to be close to His^{195} in the receptor model. This receptor showed high affinity for ANP (data not shown). Photolabeling of this mutant with iodinated pBNP1-G resulted in no peptide released by CNBr, indicating that residue 198 is not in the

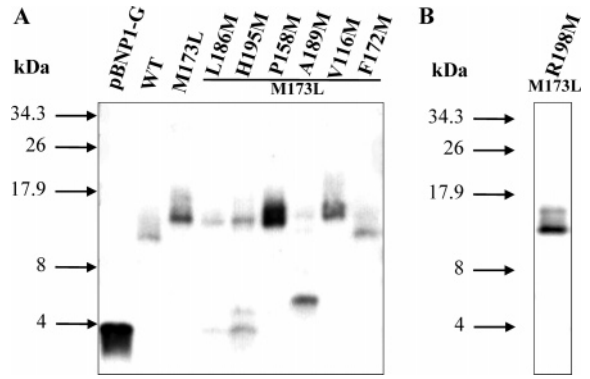

FIGURE 5: SDS−PAGE analysis of photolabeling with the pBNP1-G probe. (A) Identification of the His^{195} region. NPRA receptors were incubated with radioiodinated pBNP1-G and submitted to photoaffinity labeling as described in the Figure 1 caption. The 4 kDa band in the M173L−H195M lane is identifying the His^{195} region as a labeling site for Bpa. Results are representative of three independent experiments. (B) Identification of the Leu^{153}−Arg^{198} region. $NPRA^{M173L-R198M}$ was incubated with radioiodinated pBNP1-G and submitted to photoaffinity labeling. The 11.8 kDa band is identifying the Leu^{153}−Arg^{198} region of the receptor as a labeling site for Bpa. Results are representative of two independent experiments.

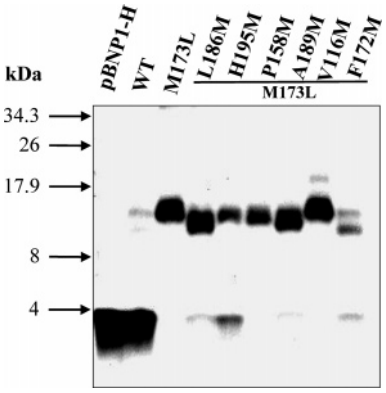

FIGURE 6: SDS−PAGE analysis of photolabeling with the pBNP1-H probe. NPRA receptors were incubated with radioiodinated pBNP1-H and submitted to photoaffinity labeling as described in the Figure 1 caption. The 4 kDa band in the WT lane identifies Met^{173} as a labeling site for Bpa. Results are representative of three independent experiments.

immediate vicinity of Phe^{26}. Nevertheless, the labeled 11.8 kDa fragment identified the Leu^{153}−Arg^{198} region. Taken together, these results indicate that Phe^{26} is binding closer to His^{195} than Arg^{198} or Leu^{186}.

Tyr^{28} of pBNP1 Binds in the Met^{173} Region. The positioning of the C-terminal tail of the peptide was also studied by use of the iodinated pBNP1-H probe. A major peptide release at 4 kDa is shown for the WT receptor (Figure 6). This identifies Met^{173} as the closest residue to Tyr^{28}. There are also minor 4 kDa bands for receptor mutants with methionine replacing His^{195}, Leu^{186}, or Phe^{172}. These observations could be due to C-terminus mobility, similar to that observed for the N-terminus of the peptide. Once again, other receptor mutants display the 10.5−13 kDa fragments that were seen with pBNP1-B, -C, and -G. This conserved pattern still pinpoints the Arg^{174}−Leu^{186} region of the receptor. However, Met^{173} is located at the edge of this region. It is then probable that a Bpa located in the mobile C-terminus of the peptide could react in the Arg^{174} and Leu^{186} region, when no methionine is exposed.

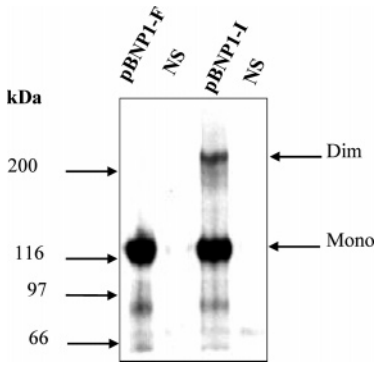

FIGURE 7: SDS−PAGE analysis of photolabeling with the pBNP1-I probe. $NPRA^{M173L}$ was incubated with radioiodinated probes (pBNP1-F and pBNP1-I) in the presence (nonspecific lane, NS) or absence of 10^{-6} M ANP and was submitted to photolabeling. The proteins were resuspended in sample buffer and directly loaded on a standard 5% gel. The positions of monomeric (Mono) and dimeric (Dim) receptors are indicated. The dimeric band resulting from pBNP1-I labeling represents 20% of the total labeled receptors. Results are representative of four independent experiments.

N-Terminus and Leu^{18} of the Peptide Interact with Opposite Receptor Subunits. Since the predicted positioning of the peptide within the binding cleft allows for its contact with both receptor subunits, we wished to identify which of the subunits of the homodimeric receptor is involved in these contact points. We thus performed photoaffinity labeling of $NPRA^{M173L}$ mutant with the dual-Bpa-substituted pBNP1-I probe. $NPRA^{M173L}$ has been selected for this experiment in order to avoid preferred reaction with methionines, which could cause Bpa to switch from one subunit to the other. $NPRA^{M173L}$ labeling with the singly substituted pBNP1-F probe was used as a control. The labeled receptors were analyzed directly on a standard SDS−5% polyacrylamide gel (Figure 7). pBNP1-I was found to yield a 230 kDa band corresponding to the dimeric receptor in addition to the 130 kDa band corresponding to the monomer. The receptor dimer band is absent in the pBNP1-F lane, confirming the specific dimerization capacity of pBNP1-I.. This experiment allowed us to quantify the proportion of dimeric and monomeric receptor. The dimeric NPRA represents 19% of the total labeled receptors. The dimeric receptor is indeed formed when both Bpa residues have formed a covalent bond. This yield of dimeric receptor is thus quite high considering that it represents the product of the incorporation yields of each Bpa individually. This result demonstrates that Leu^{18} and the N-terminus of the peptide are interacting with opposite subunits.

Molecular Modeling of the pBNP1−NPRA Complex. We first developed a model of the human NPRA in the unbound form (Figure 8A,B). Homology modeling was performed by mutating variable residues in the A-shaped rNPRA crystal structure until the predicted structure of hNPRA was obtained (*17*). The measured distance between the two Arg^{208} residues of the two monomers of the receptor was used as a probe for monitoring whether the NPRA receptor dimer was in the open, unbound state, or closed, hormone-bound state. The measured distance between the membrane-proximal lobes of the unbound form was 46 Å. We next modeled the pBNP1-bound form of hNPRA based on the current photoaffinity labeling results (Figure 8C,D), using a homology model of the NPRC−CNP crystal structure (*20*). We observed that, in the presence of pBNP1, the distance

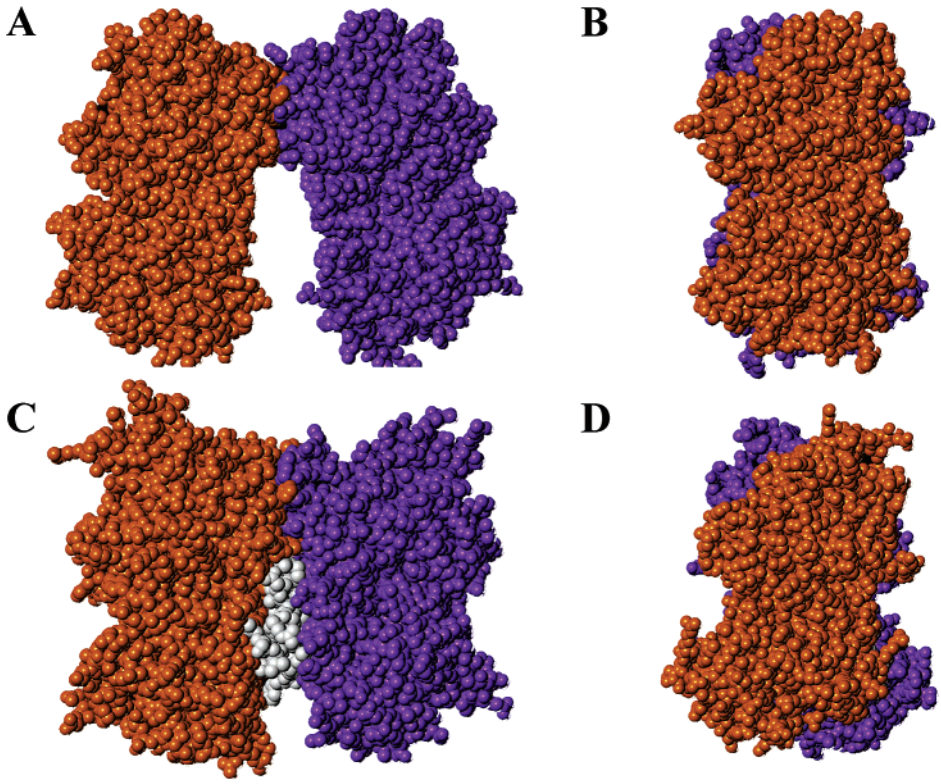

FIGURE 8: NPRA dimer models in the absence and presence of ligand. Modeling of the NPRA was carried out as described under Experimental Procedures by use of SYBYL software. (A) Front view of the open receptor. (B) Side view of the open receptor. (C) Front view of the closed peptide-bound receptor. (D) Side view of the closed peptide-bound receptor.

between the receptor subunits closes to 33 Å. The peptide also causes the membrane-proximal lobes of the receptor to twist laterally from their initial positions. Those combined hormone-induced movements could be relevant for signal transduction through the intracellular domain of the receptor. In this model the peptide is located just below the dimerization interface and is trapped between the receptor subunits. The N-terminus of the peptide seems to extend somewhat outside the binding cleft, while the C-terminus remains inside toward the opposite end of the cleft. The interactions calculated between the peptide and the receptor (Table 2) indicate that the peptide alternatively interacts with each subunit along its sequence. Some residues are also simultaneously interacting with both subunits. This suggests that peptide binding facilitates bridging the two subunits of the receptor, leading to tighter binding to the receptor dimer.

Major hydrophobic pockets were identified in the receptor binding domain. Phe^{8} and Leu^{18} of the hormone are buried in two patches and interact with many hydrophobic residues (Table 2). Residues Ser^{1}, Arg^{4}, Arg^{11}, Arg^{14}, Asn^{24}, and Arg^{27} are involved in multiple hydrogen bonds and van der Waals interactions, which secure their positions within the receptor binding cleft. Within the receptor, Phe^{165} and Met^{173} of hNPRA are the most important residues involved only in hydrophobic interactions. Tyr^{88}, Arg^{176}, and Glu^{187} provide the largest number of both hydrogen bonds and hydrophobic interactions.

According to the current model, Arg^{95} of each subunit is hydrogen-bonded to Glu^{119} of the same subunit and to Asp^{62} on the opposite side. These residues are all located at the vertex of the binding cleft. To assess the importance of these interactions, we prepared the $NPRA^{D62R}$ and $NPRA^{R95D}$ mutants and found that these mutations abrogate hormone binding (data not shown). Moreover, reversing charges with $NPRA^{D62R-R95D}$ failed to restore the binding capacity. Thus these interactions appear to be important for proper alignment of the subunits in the receptor dimer. In addition, Glu^{119} of site A is also hydrogen-bonded to Arg^{14} of the peptide, thus contributing to its binding, while the corresponding Glu^{119} in site B is free to interact in a mirror fashion if the peptide was inserted in a symmetrical position.

Molecular Dynamics of the pBNP1−NPRA Complex. We performed molecular dynamics simulations on both the bound and open forms of hNPRA with and without pBNP1 inserted into the active site. When starting with the open form of the receptor with pBNP1 attached to one of the receptor subunits, we found that within 100 ps, the receptor closed around the ligand (Figure 9A). During the remaining 200 ps simulation, the receptor fluctuated within a few angstroms of the closed form. pBNP1 was able to induce the 13 Å closure of the receptor dimer to a state equivalent to that of the closed form of hNPRA. In the absence of hormone, the open form of hNPRA remained essentially unchanged after the simulation (Figure 9B), although some fluctuation around the open form was observed. The large number of favorable electrostatic, hydrogen-bonding, and hydrophobic contacts between the hormone and receptor are necessary and essential to induce the conformational changes that allow the subunits to close from its open form to the bound state.

Molecular dynamics simulations of the closed, receptor-bound form of hNPRA were as expected. In the absence of hormone, the two subunits moved apart from each other over the first 50 ps and remained in an open state for the remainder of the simulation. In the presence of pBNP1, the receptor dimer remained in its closed state. These experiments show

Table 2: Residue Interactions in the NPRA−pBNP1 Complex

pBNP1	site A	site B
Ser[1]	R176,[2a,b] D177,[a,b] N180[a,b]	
Leu[2]	R176[b]	
Arg[3]	F172,[b] M173,[b] R176,[b] D177[2a]	
Arg[4]		F188,[b] D192,[a] L193,[b] H195,[2a,b] R198[a,b]
Ser[5]		E187,[b] R198[b]
Ser[6]	F172,[b] H185[b]	
Cys[7]	Y154,[b] F165[b]	
Phe[8]	Y154,[b] F165,[b] V168,[b] E169,[b] F172,[b] M173,[b] H185[b]	
Gly[9]	F172,[b] M173[b]	
Arg[10]	M173[b]	D192[2a]
Arg[11]	M173[b]	Y156[a,b], R157[b], P158[b], E187[a,b]
Leu[12]		Y88[b], Y156[b], P158[a]
Asp[13]	G113,[b] V116,[b] Y120[2a]	
Arg[14]	R95,[b] E119,[2a,b] Y120[a,b]	S61,[b] Y88,[b] P158,[b] G159[b]
Ile[15]	Y88,[b] F165,[b] F166[b]	
Gly[16]	Y88[b]	
Ser[17]	Y88,[b] P92[b]	A91,[b] P92,[b] R95[b]
Leu[18]	Y88[a]	V87,[b] Y88,[b] A91,[b] A111,[b] G113,[b] F114,[b] Y120,[b] F166[b]
Ser[19]	Y88,[a,b] P158,[b] D160,[b] E162[b]	F166[b]
Gly[20]		L112,[b] F165,[b] F166,[b] E169[a,b]
Leu[21]	Y156,[b] P158[b]	E169[a,b]
Gly[22]		F165,[b] E169[b]
Cys[23]	F165[b]	
Asn[24]		Y154,[b] Y156,[a,b] E187[2a,b]
Ser[25]		
Phe[26]	L186,[b] E187,[b] H195[b]	
Arg[27]	Y154,[b] Y156,[b] P158,[b] F165,[b] E187[4a,b]	
Tyr[28]		L112,[b] F172,[b] M173,[b] R176[2a]

[a] Indicates one H-bond (a number is inserted when more than one H-bond is formed). An H-bond is defined as less than or equal to 2.8 Å distance between the donor hydrogen and acceptor atom. [b] Indicates a hydrophobic or van der Waals contact. A van der Waals contact is defined as any atom between the receptor and peptide of less than or equal to 3.0 Å.

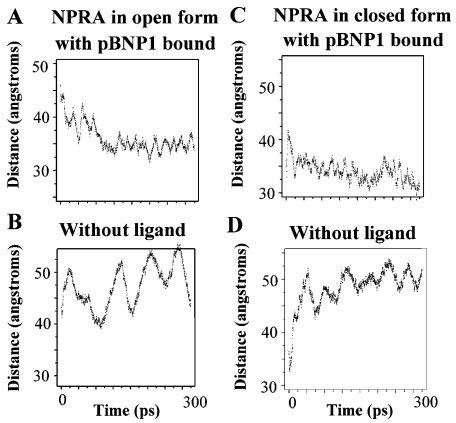

FIGURE 9: Molecular dynamics of the NPRA models. Molecular dynamics experiments were carried out as described under Experimental Procedures. (A) Open form with ligand. (B) Open form without ligand. (C) Closed form with ligand. (D) Closed form without ligand.

that the presence of hormone stabilizes the dimeric conformation of the receptor by favoring its closed state.

DISCUSSION

We have developed and validated five novel Bpa-substituted probes efficient for the mapping of the human NPRA binding site. These probes were derived from the superagonist (N,C-rANP)pBNP, named pBNP1, which displays the highest affinity reported for human NPRA (*32*). This superagonist was thus used under the assumption that it would better help to identify ligand−receptor interactions involved in high-affinity binding to human NPRA. Moreover, pBNP1 has been used as an optimal template in order to compensate for a possible loss of affinity due to Bpa substitution.

The photolabeling of the single methionine receptor mutants with pBNP1-B identified the Arg[174]−Leu[186] region as the contact point for the N-terminus of the peptide. Further investigation with pBNP1-A[1−27] and Asp-N proteinase refined this region to Asp[177]−Val[183]. This labeled fragment is centered around the N-glycosylated Asn[180] residue. These results are in agreement with the Met[173]−Phe[188] region identified by McNicoll et al. (*30*) using the [Tyr[2]]rANP [2−27] probe cross-linked by malondialdehyde at the N-terminus. The identification of a fragment instead of a major incorporation on a single methionine could be explained by the higher mobility of the N-terminal end of the peptide.

Unlike pBNP1-A and -B, the pBNP1-C probe, Bpa-substituted at Arg[3], provided a major labeling of a methionine substituted for Phe[172]. It would suggest that the mobility of the peptide chain decreases toward the ring portion of pBNP1. Nevertheless, pBNP1-C also displayed minor methionine incorporation on residues 173, 189, and 116. This observation still shows some mobility from the N-terminal tail. Those three residues are located in the vicinity of Phe[172] according to the currently proposed pBNP1-bound NPRA model. This model shows that the N-terminal tail of pBNP1 is apposed to subunit A. Arg[3] is interacting with Asp[177] of subunit A while Arg[4] is hydrogen-bonded to Asp[192] of subunit B. These ionic interactions lead us to propose an explanation for the lower affinity of pBNP1 analogues that we previously observed (*31*). pBNP amino-terminal residues Arg[6] and Asp[7] (Table 1) corresponding to Arg[3] and Arg[4] of rANP, would fail to bridge the receptor subunits through ionic interactions due to negative charge repulsion. In

addition, the corresponding residues in CNP Leu[2] and Ser[3] would also fail to provide the two positive charges, which seem to be important for high-affinity binding of natriuretic peptides. Structural documentation of the interaction of natriuretic peptides with the NPRC receptor (*20*) and recently with the rat NPRA (*23*) did not provide results concerning the amino-terminal end of those peptides. Our results with photoaffinity labeling and molecular modeling document the localization of the amino-terminal residues within the binding cleft between the receptor subunits.

Experiments with the pBNP1-F probe showed that Leu[18] strongly interacts in the vicinity of Val[116], close to Met[173]. The current model confirms that aliphatic residue Leu[18] is buried in a hydrophobic pocket located near Val[116] and Met[173] on subunit B. The CNP−NPRC structure previously reported also displays the same hydrophobic patch, which interacts with the corresponding residue Met[17] in CNP (*20*). In contrast, ANP contains the more polar residue Gln[18] at the corresponding location (*23*), a substitution that could contribute to explain the lower affinity of ANP than pBNP1 for hNPRA. The presence of a hydrophobic residue such as Leu[18] interacting with subunit B should be relevant for high-affinity binding of natriuretic peptides. It would also complement the strong interaction of Phe[8] with the hydrophobic pocket located in subunit A and most likely would contribute to stabilize the dimeric conformation of the receptor.

The results obtained with the pBNP1-G probe showed that Phe[26] is located in the His[195] neighborhood with proximity to Leu[186]. The results gathered with this probe also demonstrated the mobility of the C-terminal tail. The current model indicates that those two residues on subunit A are close to each other and to Phe[26] of the peptide. Previous photolabeling experiments with [Tyr[18],Bpa[27]]rANP[1−27] identified the Asp[191]−Arg[198] region for Arg[27] interaction (*30*). This is consistent with our positioning of the adjacent Phe[26]. Photolabeling with the pBNP1-H probe showed that Tyr[28] interacts in the Met[173] vicinity with minor labeling with residues 195, 186, and 172. Interactions near His[195] and Leu[186], which are located slightly apart from Met[173], suggest some mobility for the C-terminus as was the case for the N-terminus. In the current NPRA−pBNP1 model, Tyr[28] is close to Met[173] and Phe[172] on subunit B. Molecular modeling indicates that Phe[26] and Tyr[28] cannot interact with the same receptor subunit due to steric hindrance and should be apposed to subunits A and B, respectively (data not shown). A recent crystallographic study of truncated rANP bound to rat NPRA indicated that Phe[26] would rather interact with subunit B (*23*). However the truncated rANP used in that study is lacking all the N-terminal tail as well as Tyr[28]. Positioning of the C-terminus of such a truncated peptide is shown to correspond to that of the N-terminus in our model based on full-length pBNP1. For pBNP1, as well as for any full-length natriuretic peptide harboring both exocyclic termini, steric hindrance should constrain the N- and C-terminal ends to extend toward opposite sides of the binding cleft.

Dimerization experiments with the dual Bpa-substituted pBNP1-I probe showed that the photolabeling of the receptor with this peptide leads to the covalent dimerization of 19% of the peptide-bound receptor. This dimerization efficiency depends on the position of both Bpa residues and their individual incorporation yields. Dimerization efficiency could be estimated as the product of pBNP1-B (41%) and pBNP1-F (25%) incorporation yields if both events were independent. The dimerization incorporation yield of 19% obtained with dual Bpa-subtituted pBNP1-I is at least equal to that expected for two independent events and even higher, suggesting a concerted reaction mode for both Bpa residues of the peptide. It is then safe to conclude that the N-terminus and Leu[18] are located on opposite subunits of the receptor. Moreover, the covalent dimerization study of NPRA carried out by Rondeau et al. (*19*) using a bifunctional photoaffinity derivative of ANP substituted at each end of the peptide had also previously shown that the N- and C-termini of natriuretic peptides are interacting with opposite receptor subunits. In addition, crystallographic data of truncated rANP bound to NPRA confirmed that residue 18 of the peptide is interacting with the same hydrophobic pocket in subunit B (*23*). Taken together, these results provided a basis for generating a molecular model of the peptide bound to human NPRA.

The interactions identified between the peptide and the receptor demonstrate the importance of Tyr[154] and His[185] in the receptor. The mutation of these residues to methionine resulted in the loss of peptide binding. According to our model, Tyr[154] is interacting with four different residues of the peptide. His[185] provides interactions with two different residues in the peptide, including the conserved Phe[8]. In addition, the residue in NPRC (Ile[188]) corresponding to His[185] has been shown to be important for species specificity of peptide binding (*45*). Thus the substitution of these important residues with methionine might possibly have altered the binding interface.

The molecular modeling of both opened and closed (peptide-bound) forms of the receptor provides further confirmation for the current hypothesis for the conformational changes induced by the binding of the peptide. We observed that the binding of pBNP1 caused the subunits to twist laterally from their original positions while the membrane-proximal lobes were closing in. This observation is consistent with a dimerization study carried out with NPRA[D435C]. This mutant receptor forms a covalent disulfide bridge only when activated by ANP but remains monomeric in its basal state (*35*). The twisting of each subunit is likely to be an important conformational change that occurs in the juxtamembrane region upon receptor activation, positioning the substituted Cys[435] to form a disulfide bridge. We also observed a closing of the membrane-proximal lobes after hormone binding. According to our model, the C-terminal lobes get closer by 13 Å in the bound form. NPRC displayed the same mechanism following CNP binding, but the reported closing distance for this receptor was 20 Å. Molecular dynamics experiments also clearly showed that the presence of hormone stabilizes the dimeric conformation of the receptor by favoring its closed state. Membrane-proximal lobes moved inward in a peptide-dependent manner. In comparison, the erythropoietin receptor was shown to close by 34 Å following hormone binding (*47*, *48*). Our simulations further validate the relevance of our model for peptide-induced conformational change of the dimeric receptor molecule. This closure and twisting of the receptor subunits are both mechanisms that could lead to transmembrane signal transduction to the intracellular domain.

The recent publication of the crystal structure of rat NPRA ECD bound to truncated ANP[7−27] has shown similarities

and differences with our model. Although these authors have shown a similar rotation of each receptor monomer following peptide binding, they failed to observe any closing of the subunits (*23*). This difference with our model could be caused by the absence of TM domains and phospholipidic membrane of ECD used for crystallization. The receptor TM domains anchored in the plasma membrane present in the full-length NPRA used in the current study likely has an effect on the mobility and the positioning of the receptor subunits during activation. The truncated peptide used by Ogawa et al. (*23*) is lacking the heptameric exocyclic amino-terminus and the C-terminal residue Tyr. In addition, rANP[7−27] and the superagonist pBNP1 cyclic loops differ in terms of several potentially crucial residues. In pBNP1, Arg^{10} is replacing Gly^{10}, while Ser^{17} and Leu^{18} replace Ala^{17} and Gln^{18} (Table 1). Those residues contribute multiple interactions to both receptor subunits A and B (Table 2). Despite those differences, comparison of the residue interactions indicates that the majority of those reported by Ogawa et al. are also found in our model. In both models, the crucial residues Phe^8 and Leu^{18} (Gln^{18} in rANP) interact with the same hydrophobic pockets located on receptor subunits A and B, respectively. The major discrepancies involve the carboxy-terminal residues. For example, Leu^{21} of pBNP1 interacts with Tyr^{156} of the subunit A of human NPRA (Table 2). This residue is replaced by Asp^{156} in rat NPRA, and Leu^{21} of rANP[7−27] is interacting with Tyr^{172} of rat NPRA subunit B (*23*). Exocyclic residues Ser^{25} and Phe^{26} in rat ANP[7−27] interact with residues 187 and 198 of site B (*23*). Those residues of the receptor are instead interacting with Arg^4 and Ser^5 of pBNP1's amino-terminus. In fact, rANP[7−27] carboxy-terminus is located in a position similar to that of pBNP1 amino-terminus. Such a configuration would not be allowed if the rANP had not been truncated, since both exocyclic termini are constrained by steric exclusion. Thus the conformation and residues interactions documented for pBNP1 are likely to be more representative of intact full-length peptide. Interestingly, interaction of the last residue of rANP-[7−27] and pBNP1 involves Met^{173}, although from opposite subunits. Met^{173} from human NPRA subunit A is already interacting with Arg^3, Gly^9, Arg^{10}, and Arg^{11} of pBNP1 and thus could possibly not interact with Tyr^{28}. Thus pBNP1 carboxy-terminal interaction is likely to be preferentially with subunit B (Table 2). The presence of both Phe26 and Tyr28 in pBNP1 also constrains those two residues to interact with opposite receptor subunits. This constraint is not present for rANP[7−27], which lacks Tyr^{28} so that Phe^{26} could interact with subunit B in rat NPRA instead of subunit A as observed for pBNP1 binding to human NPRA. Some potentially crucial hydrogen-bond and ionic interactions were also documented in both models, such as Arg^{14} of peptide with Glu^{119} of site A and Asn^{24} of peptide with Glu^{187} of site B. However additional ionic interactions were apparent in our model for pBNP, such as Ser^1 and Arg^3 with residues of subunit A and Arg^4 with multiple residues of site B (Table 2). Such interactions could not be observed with the truncated form of rANP[7−27] (*23*).

Natriuretic peptides display high affinity for their receptors. This high affinity is probably caused by several strong and potentially redundant interactions. Therefore, removal or substitution of a single residue might not necessarily lead to a significant affinity decrease. Identification of those interactions that are crucial as well as those interactions with minimal impact on peptide binding might help for the development of natriuretic peptide agonists of reduced size. In this work, we used the MPA method to generate a model that provides a basis for interpreting and predicting natriuretic peptides binding to their human receptor. We presented evidence that this method could lead to a realistic binding-site structure and could facilitate the development of improved therapeutic agents.

REFERENCES

1. Espiner, E. A., Richards, A. M., Yandle, T. G., and Nicholls, M. G. (1995) Natriuretic hormones, *Endocrinol. Metab. Clin. North Am. 24*, 481−509.
2. Drewett, J. G., and Garbers, D. L. (1994) The family of guanylyl cyclase receptors and their ligands, *Endocr. Rev. 15*, 135−162.
3. D'Souza, S. P., Davis, M., and Baxter, G. F. (2004) Autocrine and paracrine actions of natriuretic peptides in the heart, *Pharmacol. Ther. 101*, 113−129.
4. Itoh, H., Pratt, R. E., and Dzau, V. J. (1990) Atrial natriuretic polypeptide inhibits hypertrophy of vascular smooth muscle cells, *J. Clin. Invest. 86*, 1690−1697.
5. Cao, L., and Gardner, D. G. (1995) Natriuretic peptides inhibit DNA synthesis in cardiac fibroblasts, *Hypertension 25*, 227−234.
6. Chinkers, M., and Garbers, D. L. (1991) Signal transduction by guanylyl cyclases, *Annu. Rev. Biochem. 60*, 553−575.
7. Iyengar, S., Feldman, D. S., Trupp, R., and Abraham, W. T. (2004) Nesiritide for the treatment of congestive heart failure, *Expert Opin. Pharmacother. 5*, 901−907.
8. Lucas, K. A., Pitari, G. M., Kazerounian, S., Ruiz-Stewart, I., Park, J., Schulz, S., Chepenik, K. P., and Waldman, S. A. (2000) Guanylyl cyclases and signaling by cyclic GMP, *Pharmacol. Rev. 52*, 375−414.
9. Sudoh, T., Minamino, N., Kangawa, K., and Matsuo, H. (1990) C-type natriuretic peptide (CNP): a new member of natriuretic peptide family identified in porcine brain, *Biochem. Biophys. Res. Commun. 168*, 863−870.
10. Suga, S., Nakao, K., Hosoda, K., Mukoyama, M., Ogawa, Y., Shirakami, G., Arai, H., Saito, Y., Kambayashi, Y., Inouye, K., and Imura, H. (1992) Receptor selectivity of natriuretic peptide family, atrial natriuretic peptide, brain natriuretic peptide, and C-type natriuretic peptide, *Endocrinology 130*, 229−239.
11. Koller, K. J., Lowe, D. G., Bennett, G. L., Minamino, N., Kangawa, K., Matsuo, H., and Goeddel, D. V. (1991) Selective activation of the B natriuretic peptide receptor by C-type natriuretic peptide (CNP), *Science 252*, 120−123.
12. Maack, T. (1992) Receptors of atrial natriuretic factor, *Annu. Rev. Physiol. 54*, 11−27.
13. Potter, L. R., and Hunter, T. (2001) Guanylyl cyclase-linked natriuretic peptide receptors: structure and regulation, *J. Biol. Chem. 276*, 6057−6060.
14. Fuller, F., Porter, J. G., Arfsten, A. E., Miller, J., Schilling, J. W., Scarborough, R. M., Lewicki, J. A., and Schenk, D. B. (1988) Atrial natriuretic peptide clearance receptor. Complete sequence and functional expression of cDNA clones, *J. Biol. Chem. 263*, 9395−9401.
15. Anand-Srivastava, M. B., Gutkowska, J., and Cantin, M. (1991) The presence of atrial-natriuretic-factor receptors of ANF-R2 subtype in rat platelets. Coupling to adenylate cyclase/cyclic AMP signal-transduction system, *Biochem. J. 278*, 211−217.
16. Murthy, K. S., Teng, B. Q., Zhou, H., Jin, J. G., Grider, J. R., and Makhlouf, G. M. (2000) G(i-1)/G(i-2)-dependent signaling by single-transmembrane natriuretic peptide clearance receptor, *Am. J. Physiol. Gastrointest. Liver Physiol. 278*, 974−980.
17. van den Akker, F., Zhang, X., Miyagi, M., Huo, X., Misono, K. S., and Yee, V. C. (2000) Structure of the dimerized hormone-binding domain of a guanylyl-cyclase-coupled receptor, *Nature 406*, 101−104.
18. Misono, K. S., Sivasubramanian, N., Berkner, K., and Zhang, X. (1999) Expression and purification of the extracellular ligand-binding domain of the atrial natriuretic peptide (ANP) receptor: monovalent binding with ANP induces 2:2 complexes, *Biochemistry 38*, 516−523.

19. Rondeau, J. J., McNicoll, N., Gagnon, J., Bouchard, N., Ong, H., and De Léan, A. (1995) Stoichiometry of the atrial natriuretic factor−R1 receptor complex in the bovine zona glomerulosa, *Biochemistry 34*, 2130−2136.
20. He, X., Chow, D.-c., Martick, M. M., and Garcia, K. C. (2001) Allosteric activation of a spring-loaded natriuretic peptide receptor dimer by hormone, *Science 293*, 1657−1662.
21. De Léan, A., McNicoll, N., and Labrecque, J. (2003) Natriuretic peptide receptor A activation stabilizes a membrane-distal dimer interface, *J. Biol. Chem. 278*, 11159−11166.
22. Qiu, Y., Ogawa, H., Miyagi, M., and Misono, K. S. (2004) Constitutive activation and uncoupling of the atrial natriuretic peptide receptor by mutations at the dimer interface. Role of the dimer structure in signaling, *J. Biol. Chem. 279*, 6115−6123.
23. Ogawa, H., Qiu, Y., Ogata, C. M., and Misono, K. S. (2004) Crystal structure of hormone-bound atrial natriuretic peptide receptor extracellular domain: Rotation mechanism for transmembrane signal transduction, *J. Biol. Chem. 279*, 28625−28631.
24. Dorman, G., and Prestwich, G. D. (1994) Benzophenone photophores in biochemistry, *Biochemistry 33*, 5661−5673.
25. Rihakova, L., Deraet, M., Auger-Messier, M., Perodin, J., Boucard, A. A., Guillemette, G., Leduc, R., Lavigne, P., and Escher, E. (2002) Methionine proximity assay, a novel method for exploring peptide ligand−receptor interaction, *J. Recept. Signal Transduct. Res. 22*, 297−313.
26. Kage, R., Leeman, S. E., Krause, J. E., Costello, C. E., and Boyd, N. D. (1996) Identification of methionine as the site of covalent attachment of a p-benzoyl-phenylalanine-containing analogue of substance P on the substance P (NK-1) receptor, *J. Biol. Chem. 271*, 25797−25800.
27. Servant, G., Laporte, S. A., Leduc, R., Escher, E., and Guillemette, G. (1997) Identification of angiotensin II-binding domains in the rat AT2 receptor with photolabile angiotensin analogues, *J. Biol. Chem. 272*, 8653−8659.
28. Laporte, S. A., Boucard, A. A., Servant, G., Guillemette, G., Leduc, R., and Escher, E. (1999) Determination of peptide contact points in the human angiotensin II type I receptor (AT1) with photosensitive analogues of angiotensin II, *Mol. Endocrinol. 13*, 578−586.
29. McNicoll, N., Escher, E., Wilkes, B. C., Schiller, P. W., Ong, H., and De Léan, A. (1992) Highly efficient photoaffinity labeling of the hormone binding domain of atrial natriuretic factor receptor, *Biochemistry 31*, 4487−4493.
30. McNicoll, N., Gagnon, J., Rondeau, J. J., Ong, H., and De Léan, A. (1996) Localization by photoaffinity labeling of natriuretic peptide receptor-A binding domain, *Biochemistry 35*, 12950−12956.
31. Mimeault, M., Fournier, A., Féthière, J., and De Léan, A. (1993) Development of natriuretic peptide analogues selective for the atrial natriuretic factor-R1A receptor subtype, *Mol. Pharmacol. 43*, 775−782.
32. Bodart, V., Rainey, W. E., Fournier, A., Ong, H., and De Léan, A. (1996) The H295R human adrenocortical cell line contains functional atrial natriuretic peptide receptors that inhibit aldosterone biosynthesis, *Mol. Cell. Endocrinol. 118*, 137−144.
33. Coupal, M., De Léan, A., McNicoll, N., and Fournier, A. (1999) Development of p-benzoylbenzoylated [N,C,rANP(1−28)]pBNP32 (pBNP1) derivatives and affinity photolabeling of the bovine NPR-A receptor, *Biochem. Biophys. Res. Commun. 258*, 81−86.
34. Bovy, P. R. (1990) Structure activity in the atrial natriuretic peptide (ANP) family, *Med. Res. Rev. 10*, 115−142.
35. Li, B., Tom, J. Y., Oare, D., Yen, R., Fairbrother, W. J., Wells, J. A., and Cunningham, B. C. (1995) Minimization of a polypeptide hormone, *Science 270*, 1657−1660.
36. Carpenter, K. A., Wilkes, B. C., De Léan, A., Fournier, A., and Schiller, P. W. (1997) Hydrophobic forces are responsible for the folding of a highly potent natriuretic peptide analogue at a membrane mimetic surface: an NMR study, *Biopolymers 42*, 37−48.
37. Fairbrother, W. J., McDowell, R. S., and Cunningham, B. C. (1994) Solution conformation of an atrial natriuretic peptide variant selective for the type A receptor, *Biochemistry 33*, 8897−8904.
38. Lia, F., Rajotte, D., Clark, S. C., and Hoang, T. (1996) A dominant negative granulocyte-macrophage colony-stimulating factor receptor alpha chain reveals the multimeric structure of the receptor complex, *J. Biol. Chem. 271*, 28287−28293.
39. Labrecque, J., Deschênes, J., McNicoll, N., and De Léan, A. (2001) Agonistic induction of a covalent dimer in a mutant of natriuretic peptide receptor-A documents a juxtamembrane interaction that accompanies receptor activation, *J. Biol. Chem. 276*, 8064−8072.
40. Merrifield, R. B. (1963) Solid-Phase Peptide Synthesis. I. The Synthesis of a Tetrapeptide, *J. Am. Chem. Soc. 85*, 2149−2154.
41. Kaiser, E., Colescott, R. L., Bossinger, C. D., and Cook, P. I. (1970) Color test for detection of free terminal amino groups in the solid-phase synthesis of peptides, *Anal. Biochem. 34*, 595−598.
42. Labrecque, J., McNicoll, N., Marquis, M., and De Léan, A. (1999) A disulfide-bridged mutant of natriuretic peptide receptor-A displays constitutive activity. Role of receptor dimerization in signal transduction, *J. Biol. Chem. 274*, 9752−9759.
43. De Léan, A., Munson, P. J., and Rodbard, D. (1978) Simultaneous analysis of families of sigmoidal curves: application to bioassay, radioligand assay, and physiological dose−response curves, *Am. J. Physiol. 235*, E97−E102.
44. Schagger, H., and von Jagow, G. (1987) Tricine-sodium dodecyl sulfate-polyacrylamide gel electrophoresis for the separation of proteins in the range from 1 to 100 kDa, *Anal. Biochem. 166*, 368−379.
45. van den Akker, F. (2001) Structural insights into the ligand binding domains of membrane bound guanylyl cyclases and natriuretic peptide receptors, *J. Mol. Biol. 311*, 923−937.
46. Miyagi, M., Zhang, X., and Misono, K. S. (2000) Glycosylation sites in the atrial natriuretic peptide receptor: oligosaccharide structures are not required for hormone binding, *Eur. J. Biochem. 267*, 5758−5768.
47. Syed, R. S., Reid, S. W., Li, C., Cheetham, J. C., Aoki, K. H., Liu, B., Zhan, H., Osslund, T. D., Chirino, A. J., Zhang, J., Finer-Moore, J., Elliott, S., Sitney, K., Katz, B. A., Matthews, D. J., Wendoloski, J. J., Egrie, J., and Stroud, R. M. (1998) Efficiency of signaling through cytokine receptors depends critically on receptor orientation, *Nature 395*, 511−516.
48. Livnah, O., Stura, E. A., Middleton, S. A., Johnson, D. L., Jolliffe, L. K., and Wilson, I. A. (1999) Crystallographic evidence for preformed dimers of erythropoietin receptor before ligand activation, *Science 283*, 987−990.
49. Engel, A. M., and Lowe, D. G. (1995) Characterization of the hormone binding site of natriuretic peptide receptor-C, *FEBS Lett. 360*, 169−172.

BI048251Y